ACTA ACUSTICA UNITED WITH ACUSTICA
Vol. 89 (2003) 586 – 594

An Experimental Facility for Measurement of Acoustic Transmission Matrix and Acoustic Power Dissipation of Duct Discontinuity in Higher Order Modes Propagation Conditions

Azzedine Sitel, Jean-Michel Ville, Félix Foucart
Laboratoire Roberval UMR UTC-CNRS no.6066, Université de Technologie de Compiègne, BP 20529, F-60205 Compiègne cedex, France

Summary
An original experimental facility for measuring acoustic transmission matrices of duct discontinuities is described. It is an extension of a previous method developed for measuring reflection matrices and based on measurement of acoustic pressure in two closed cross sections which separates incident and reflected modes after a modal decomposition by a Fourier-Lommel's transform. In the new facility, the discontinuity is located between two measurement duct elements, and the entire experiment is automatic and controlled by a working station. The formulations and the flow diagram of the specific data treatment procedure which are performed to determine the reflection and transmission matrices' coefficients, the axial acoustic intensity per mode and total acoustic powers are described in detail. An experiment with a hard wall duct test section without any discontinuity was conducted. Results of reflection and transmission matrices, acoustic powers and intensities are discussed.

PACS no. 43.20.Mv

1. Introduction

To optimize and design new concepts for reducing noise radiated by inlets of turbomachines or aircraft engines, a thorough understanding and an accurate description of sound propagation in ducts through discontinuities are necessary [1]. A reliable experiment can contribute to reaching this goal. For plane acoustic wave propagation conditions, many works [2, 3] have already been done in developing experimental methods to characterize these discontinuities. For higher order modes' propagation conditions, an extension of the two microphones technique was investigated [4]. It was applied to the measurement of acoustic reflection matrix coefficients of an inlet and successfully compared with theoretical results [5].

The study presented in this paper is an extension of this previous work [5] on the measurement of the transmission matrix of a discontinuity. It is a step on the way to a more complete characterization of discontinuity by scattering or transfer matrices [6]. The pressure distributions measured in two closed cross sections before and after the discontinuity by two pairs of microphones are Fourier Lommel's transformed, then N incident and reflected cut-on modes are separated. Computations of the NxN coefficients of reflection matrices on both sides of the discontinuity and of the transmission matrix are performed after a process of generation of N independent incident fields. Also, acoustic powers in cross sections before and after the discontinuity are deduced. The total and per mode acoustic power attenuations of the discontinuity are measured.

Received 12 December 2002,
accepted 31 March 2003.

2. Theory

2.1. Description of the sound field in the duct

Consider a discontinuity located between two circular elements of a cylindrical duct of radius a with hard wall (Figure 1). In no flow conditions, the fluid is assumed to be ideal and linear acoustic theory to be valid. Then, the acoustic pressure distribution in the duct is written in cylindrical coordinates (r, θ, z) as [7]:

$$p(r,\theta,z,t) = \sum_{m=-\infty}^{+\infty} \sum_{n=0}^{\infty} P_{mn}(z)\psi_{mn}(r,\theta)\,\mathrm{e}^{-\mathrm{i}\omega t}. \qquad (1)$$

The eigenfunctions ψ_{mn} are given by

$$\psi_{mn}(r,\theta) = J_m\left(\frac{\chi_{mn}}{a}\right)\mathrm{e}^{\mathrm{i}m\theta}. \qquad (2)$$

The total modal coefficients P_{mn} in a cross section located at axial coordinate z are:

$$P_{mn}(z) = \left[A^i_{mn}\mathrm{e}^{\mathrm{i}k_{mn}z} + A^r_{mn}\mathrm{e}^{-\mathrm{i}k_{mn}z}\right], \qquad (3)$$

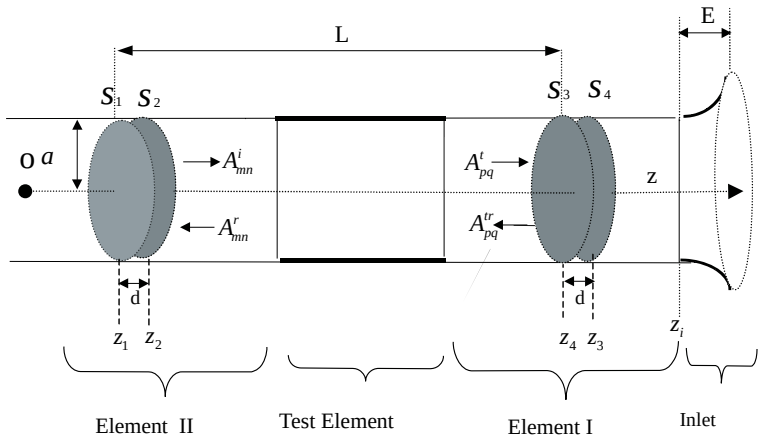

Figure 1. Duct configuration diagram. S_1, S_2: Measurement cross sections (element II), S_3, S_4: Measurement cross sections (element I). $L = z_3 - z_1 = 100$ cm, $d = 12$ mm, $a = 7.5$ cm, $E = 4.8$ cm.

where A^i_{mn}, A^r_{mn} and A^t_{mn}, A^{tr}_{mn} are deduced in $z = 0$ from measurements, respectively, in the duct element II and I.

2.2. Computation of the incident and reflected modal coefficients

Assuming, for each frequency f, that in the duct element II, the total acoustic pressure distributions p_1 and p_2 are known as a function of r and θ in two closed cross sections located at z_1 and z_2 (Figure 1), the coefficients A^i_{mn} and A^r_{mn} are calculated in two steps:

- p_1 and p_2 are Fourier Lommel's transformed [8] to get modal coefficients $P_{mn}(z_1)$ and $P_{mn}(z_2)$
- A^i_{mn} and A^r_{mn} are deduced from the relationship

$$\begin{Bmatrix} A^i_{mn} \\ A^r_{mn} \end{Bmatrix} = M^{-1}_{mn} \begin{Bmatrix} P_{mn}(z_1) \\ P_{mn}(z_2) \end{Bmatrix}, \tag{4}$$

where

$$M_{mn} = \begin{bmatrix} \mathrm{e}^{\mathrm{i}k_{mn}z_1} & \mathrm{e}^{-\mathrm{i}k_{mn}z_1} \\ \mathrm{e}^{\mathrm{i}k_{mn}z_2} & \mathrm{e}^{-\mathrm{i}k_{mn}z_2} \end{bmatrix}. \tag{5}$$

Equation 4 has solutions if $\det[M_{mn}] \neq 0$: $d \neq q(\lambda_{mn}/2)$, $q = 1, 2, 3 \ldots$. As the plane wave wavelength is the smallest among all modes, this condition on distance d between both cross sections located in z_1 and z_2 (or in z_3 and z_4) leads to a definition of an upper limit to the frequency domain [9]:

$$f < f_{\max} = \frac{2c}{5d}. \tag{6}$$

2.3. Computation of the reflection and transmission matrices coefficients

2.3.1. Reflection matrix [R]

If the duct can be regarded as a linear, time invariant and passive system in the positive z direction, a linear relationship [4] between A^i_{mn} and A^r_{mn} exists:

$$A^r_{mn} = R_{mn,mn} A^i_{mn} + \sum_{mn \neq pq} R_{mn,pq} A^i_{pq}. \tag{7}$$

$R_{mn,mn}$ and $R_{mn,pq}$ are calculated in $z = 0$. In duct element II, these coefficients depend on the discontinuity and on the load conditions downstream from the discontinuity. Assuming that N incident acoustic pressure fields are generated, the N^2 coefficients $R_{mn,pq}$ are solutions of the following system:

$$[R] = [A^r][A^i]^{-1}. \tag{8}$$

A column j of $[A^i]$ is filled with terms $A^{i,j}_{mn}$ which represent the amplitudes of modes (m, n) issued from the jth configuration of incident field. If the N incident fields are linearly independent, the matrix $[A^i]$ is reversible.

These operations can be applied to data issued from measurements in both sections located on each side of the discontinuity. $[R^I]$ is defined as the reflection matrix measured in the duct element located near the inlet and $[R^{II}]$ is the reflection matrix measured in the duct element located near the source (Figure 1 and Figure 2).

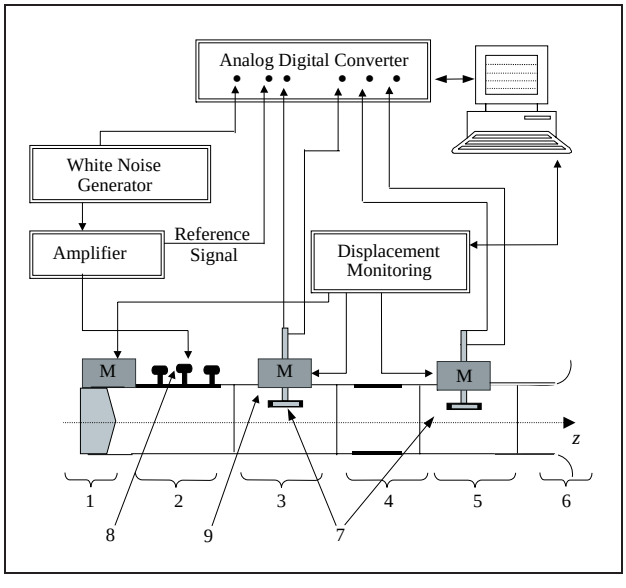

Figure 2. Experimental setup. 1: Absorbing foam, 2: source element, 3: measurement element II, 4: test element, 5: measurement element I, 6: duct inlet, 7: sound intensity probe, 8: sources, 9: step by step motors.

2.3.2. Transmission Matrix [T]

Assuming a linear relationship between A^t_{mn} and A^i_{mn}, acoustic transmission through the discontinuity is defined by:

$$A^t_{mn} = T_{mn,mn}A^i_{mn} + \sum_{mn\neq pq} T_{mn,pq}A^i_{pq}. \qquad (9)$$

$T_{mn,mn}$ and $T_{mn,pq}$ are calculated in $z = 0$. These coefficients depend on the discontinuity and on the load conditions downstream from this discontinuity. Usually the transmission coefficient is defined with an anechoic duct termination. If the N acoustic pressure fields produced are linearly independent, the $N^2 T_{mn,pq}$ coefficients are solutions of the system

$$[T] = [A^t][A^i]^{-1}. \qquad (10)$$

2.3.3. Acoustic Power and attenuation

For each source configuration, the incident and reflected modal coefficients on each side of the discontinuity are known. The modal coefficients P_{mn} of acoustic pressure are deduced from equation (3) and the modal coefficients $V_{z,mn}$ of axial acoustic particle velocity are deduced from

$$V_{z,mn} = \frac{k_{mn}}{\rho c k}\left[A^i_{mn}\mathrm{e}^{\mathrm{i}k_{mn}z} - A^r_{mn}\mathrm{e}^{-\mathrm{i}k_{mn}z}\right]. \qquad (11)$$

The total acoustic power computation is performed by adding cut-on modes' intensities:

$$W = \sum_{m=-\mu}^{+\mu}\sum_{n=0}^{\nu} I_{z,mn}N_{mn}, \qquad (12)$$

where $$N_{mn} = SJ^2_m(\chi_{mn})\left(1 - \frac{m^2}{\chi^2_{mn}}\right) \qquad (13)$$

is the normalization factor, the axial component of acoustic intensity of mode (m, n) is defined by

$$I_{z,mn} = \frac{1}{2}\Re e\{P_{mn}V^*_{z,mn}\}. \qquad (14)$$

Acoustic powers are calculated from modal coefficients A^i_{mn} and A^r_{mn} in duct element II and from A^t_{mn} and A^{tr}_{mn} in duct element I with the following relationships:

$$W^I = \sum_{m=-\mu}^{+\mu}\sum_{n=0}^{\nu} N_{mn}\frac{k_{mn}}{2\rho c}\left(|A^i_{mn}|^2 - |A^r_{mn}|^2\right), \qquad (15)$$

$$W^{II} = \sum_{m=-\mu}^{+\mu}\sum_{n=0}^{\nu} N_{mn}\frac{k_{mn}}{2\rho c}\left(|A^t_{mn}|^2 - |A^{tr}_{mn}|^2\right). \qquad (16)$$

The level of attenuation (dB) due to the discontinuity is given by

$$\Delta W = 10\log_{10}\left(\frac{W^{II}}{W^I}\right). \qquad (17)$$

As the result is independent of the source configuration and because N experiments are available, the mean value $\overline{\Delta W}$ and the standard deviation $\sigma(\Delta W)$ are computed. An estimation of the effect of the source configuration on the result of the attenuation is therefore available,

$$\overline{\Delta W} = \frac{1}{N}\sum_{n=1}^{N}\Delta W_n, \qquad (18)$$

$$\sigma(\Delta W) = \sqrt{\overline{\Delta W^2} - \overline{\Delta W}^2} \qquad (19)$$

$$\overline{\Delta W^2} = \frac{1}{N}\sum_{n=1}^{N}\Delta W_n^2. \qquad (20)$$

3. Measurement of $[R]$ and $[T]$ matrices

To perform the measurements of the transmission matrix of the discontinuity and of the acoustic power attenuation produced, a new facility was built. A measurement duct element was added and specific process developed to compute $[T]$ and acoustic powers. The entire experimental procedure of data collection was monitored by a workstation.

3.1. Hardware

The facility, which was built under a grant with E.E.C [1], is installed in the anechoic chamber of the University of Compiegne. The equipment is made of five duct components (0.5 m long and 0.15 m diameter) and of an inlet (Figure 2):

1. Absorbent element to avoid reflection.
2. The source section with three acoustic drivers flush mounted in a z line. The distance between each is 0.15 m. This entire section can rotate over 360°.
3. The measurement duct element II with a radial boom and a B&K sound intensity probe attached at its end. It is directed toward the z axis and the 1/4-inch microphones are 0.012 m apart. According to equation (6), the frequency has to be lower than 11000 Hz. This entire section can rotate over 360°.
4. The discontinuity to be tested.
5. The measurement duct element I identical to the duct element II. The distance L between measurement cross sections located in duct elements I and II is 1 m.
6. The inlet designed to fill an aerodynamic function.

Angular and radial displacements are provided by step-by-step motors. A working station automatically operates rotation of the source section, choice of the axial source, and displacements of the probe in the r direction (15 positions) and in the θ direction (16 positions). It also supplies the white noise generation to sources from 0 to 3000 Hz and the acquisition through an analog-digital converter of the signals issued from the 4 microphones.

3.2. Experimental procedure

The experimental procedure is divided in two steps:

- Collection of the transfer functions between microphones and reference signals issued from the generator in the 4 cross sections at 240 points and for N source configurations.
- Processing of collected data.

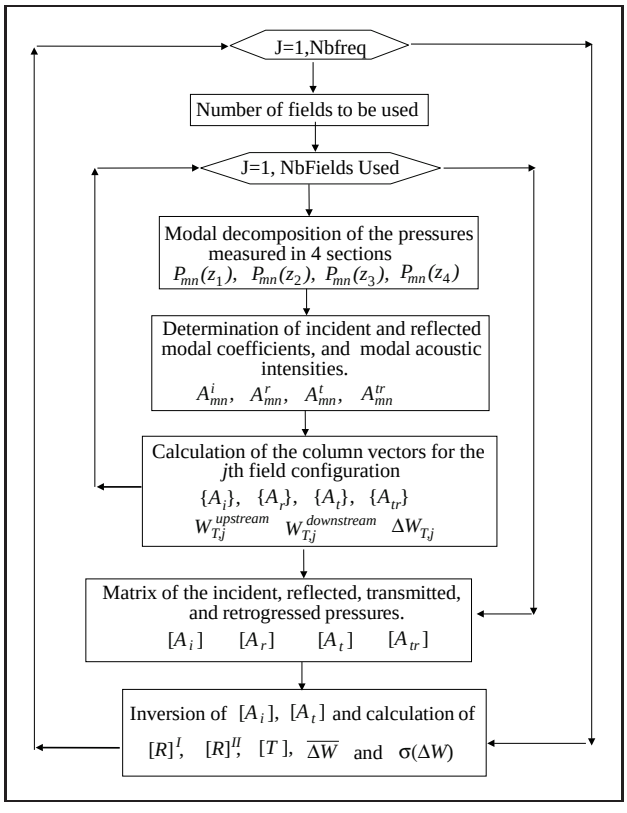

Figure 3. Flow chart of the data processing.

Table I. The experimental source configurations.

Source Configuration No.	θ (°)	z (cm)
1	0	0
2	120	15
3	240	15
4	45	0
5	165	15
6	285	15

Table II. The modal lower ka limits.

(m,n)	$(0,0)$	$(\pm1,0)$	$(\pm2,0)$	$(0,1)$
Theoretical ka	0	1.84	3.05	3.83
Measured ka	0	1.9	3.11	3.9
Lower limit ka	0.4	1.94	3.15	3.92

3.2.1. Data collection

Measurements are performed for a total wave number ka variation from 0 to 4. A maximum $N = 6$ modes are cut-on: $(0,0)$; $(\pm1,0)$; $(\pm2,0)$; $(0,1)$. For each of the 240 points in the 4 cross sections and for each microphone, the transfer function between the generator and microphone signals provide, after calibration, the amplitude and phase of the local acoustic pressure normalized by the level of the generator. The origin of the z axis (Figure 1) is then given by the reference phase that is in the source z axis position.

To compute the 36 coefficients of $[R]$ and $[T]$ matrices, 6 linearly independent incident acoustic fields have to be set up. During a previous study [5], it was shown that moving the source in θ or z direction depending on the acoustic pressure modal distribution ensures generation of these independent acoustic fields. In Table I, the source coordinates used for each of the 6 configurations are given.

3.2.2. Data processing

For each source configuration, signals are post processed as shown on the flow chart described in Figure 3. As a cross section is divided into 16 positions in the θ direction, the azimuthal wave number spectrum is computed for $m = -7$ to $+7$ [8]. The calculations of matrices $[R]$, equation (8) and $[T]$, equation (10), are performed with a "selective" method [5] where the size N of the matrix is suited to the frequency, N being the number of cut-on modes.

3.3. Results

The results presented in this paper were obtained with a hard wall test duct without any discontinuity. The purpose of this experiment was to validate the procedure and to estimate uncertainties.

3.3.1. Results of the measurement of the matrices $[R^I]$ and $[R^{II}]$

As there is no discontinuity and according to equation (8), all the complex coefficients $R_{mn,pq}$ for both duct elements I and II are calculated in $z = 0$, the coefficients on the diagonals of matrices $[R^I]$ and $[R^{II}]$ are theoretically equal in modulus and phase. Results including mode $(0,1)$ are not included in this analysis because its cut-on frequency is too close of the upper limit of the frequency domain of study. All the coefficients located outside of the diagonals are in theory equal to zero because the duct geometry is axi-symetric and then no conversion between azimuthal modes can occur.

Results of the modulus of $R^I_{00,00}$ and $R^{II}_{00,00}$ are presented in Figure 4. Both curves are close. Near the cut-off frequency of a mode, as the distance d between microphones is small compared with the modal axial wavelength, results become critical. A condition between d and λ_{mn} was determined in previous works [5, 9]:

$$d/\lambda_{mn} \geq 0.05. \tag{21}$$

Applying this condition to the plane wave mode $(0,0)$ with $d = 0.012$ m leads to a ka limit equal to 0.98, which is obviously too high with regard to the experimental result of $R^I_{00,00}$ (Figure 4). The use of a sound intensity probe which avoids oscillations put down to probe diffraction in a previous work [5] allows, in addition, the reduction of the ka limit to 0.4 as pointed out in Figure 4. Therefore a new condition for any mode (m,n) can be deduced:

$$d/\lambda_{mn} \geq 0.01. \tag{22}$$

The ka limits which satisfy the condition equation (22) are indicated for each mode in Table II and will be marked on

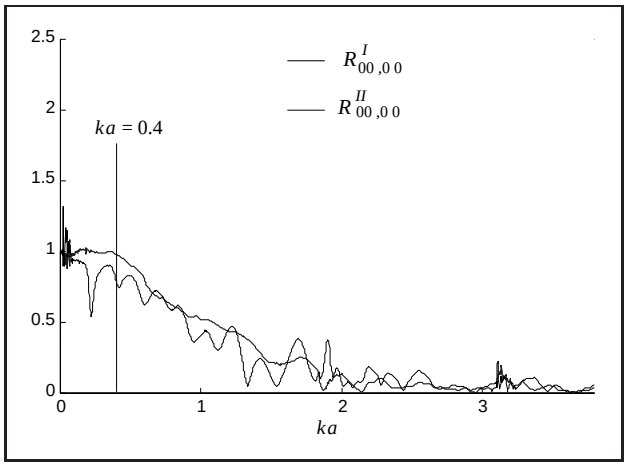

Figure 4. Modulus of reflection coefficients of plane wave mode $R^{I}_{00,00}$ and $R^{II}_{00,00}$ versus ka.

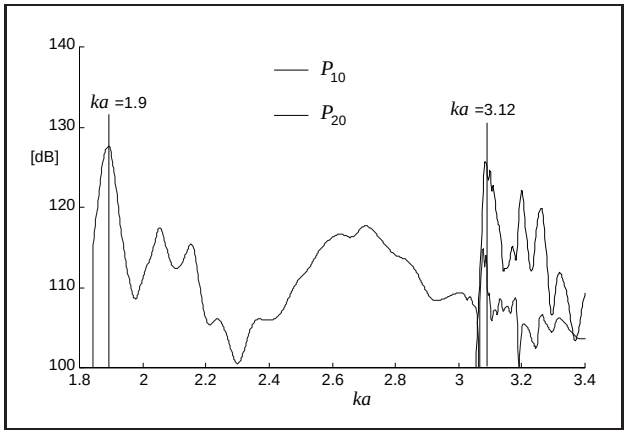

Figure 5. Modal coefficients in cross section $z = z_4$.

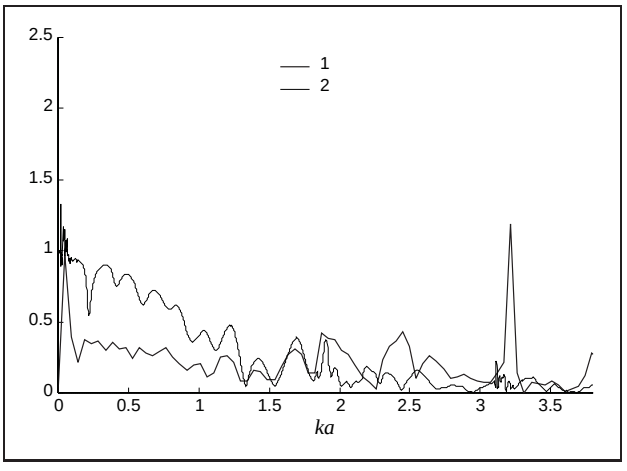

Figure 6. Influence of the filter frequency bandwidth Δf on $R^{II}_{00,00}$ (1: 35 Hz; 2: 1.54 Hz).

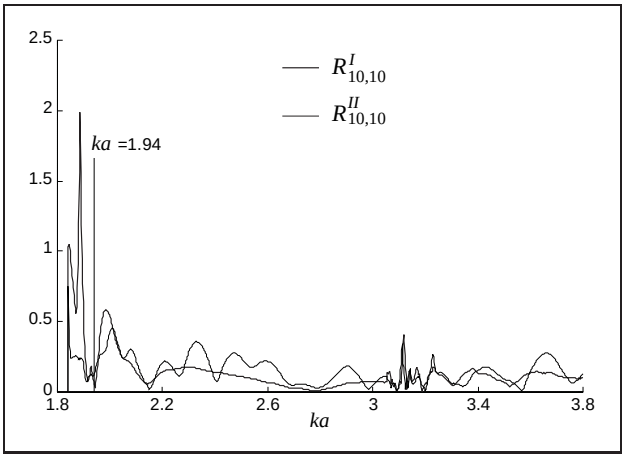

Figure 7. Modulus of reflection coefficients of mode $(1,0)$ $R^{I}_{10,10}$ and $R^{II}_{10,10}$ versus ka.

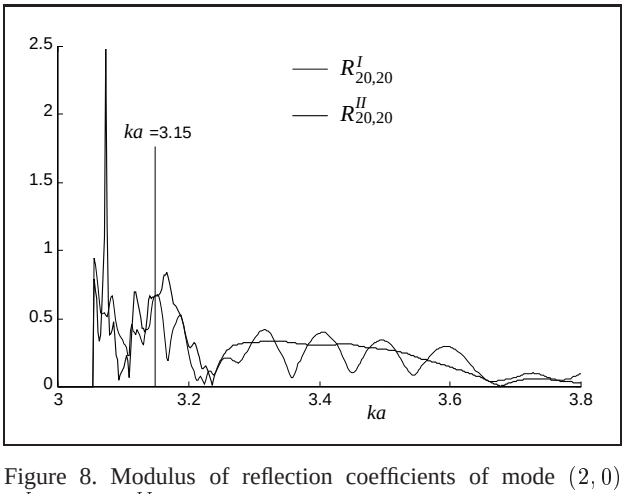

Figure 8. Modulus of reflection coefficients of mode $(2,0)$ $R^{I}_{20,20}$ and $R^{II}_{20,20}$ versus ka.

all curves. These limits are computed taking into account that actual ka cut-off values are slightly different from the theoretical ones as pointed out by Figure 5.

Values of the modulus of $R^{I}_{00,00}$ and $R^{II}_{00,00}$ are different for some frequencies where pressure nodes occur on microphones. The values of these pressure node frequencies depend on the distance between the microphone and the inlet. Because this distance is longer for element II than for element I, the effect on $R^{II}_{00,00}$ is much more critical. An improvement of the results was obtained by reducing the filter bandwidth of analysis with an increase in the number of samples during the acquisition process as shown in Figure 6. Better results would also have been achieved by reducing reflection on the inlet [10]. A gap which was already observed in [5] occurs on results at modes' cut-off frequencies.

Results of the modulus of $R^{I}_{10,10}$ and $R^{II}_{10,10}$ and $R^{I}_{20,20}$ and $R^{II}_{20,20}$ are presented respectively in Figure 7 and Figure 8. The same comments as for the plane wave case can be done. The values of $R^{I,II}_{10,10}$ and $R^{I,II}_{20,20}$ are decreasing when increasing ka from the cut-on frequency.

The phases of $R^{I}_{00,00}$ and $R^{II}_{00,00}$ plotted in Figure 9 versus ka were translated to z_I, the axial location before the inlet cross section increases. The slope of the phase curve corresponds to about two times the distance $E = 4.8\,\text{cm}$ between the inlet face and z_I.

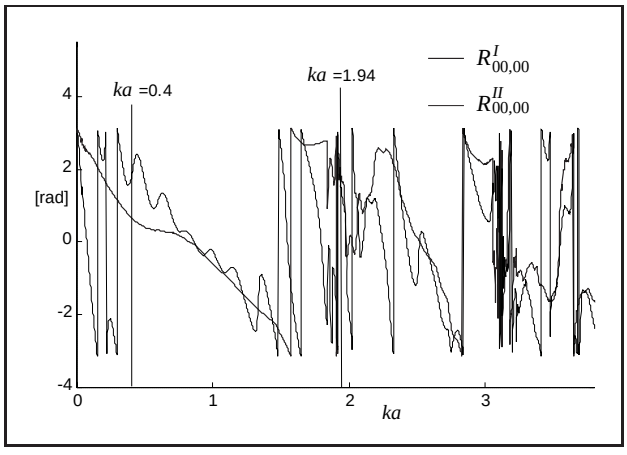

Figure 9. Phase of reflection coefficients of plane wave mode $R^I_{00,10}$ and $R^{II}_{00,00}$ versus ka in $z = z_I$.

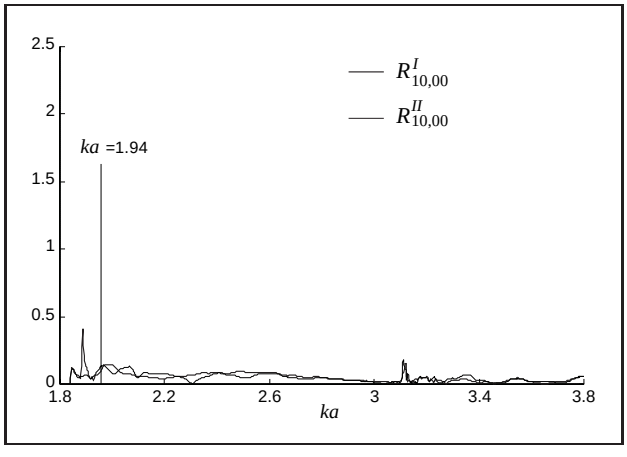

Figure 10. Modulus of conversion coefficients $R^I_{10,00}$ and $R^{II}_{10,00}$ versus ka.

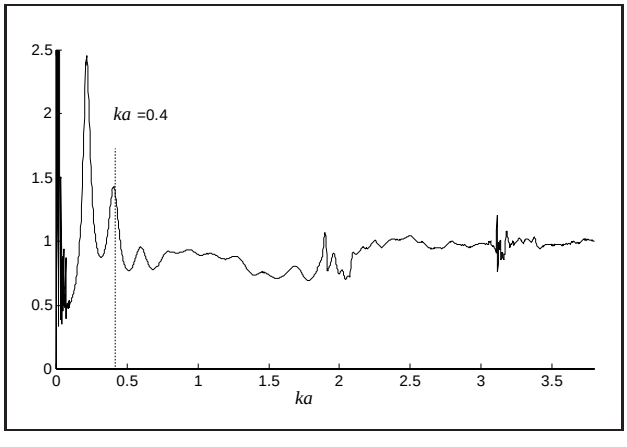

Figure 11. Modulus of the plane wave transmission coefficient $T_{00,00}$ versus ka.

Results of the modulus of the conversion coefficients $R^I_{10,00}$ and $R^{II}_{10,00}$ of mode $(0,0)$ into mode $(1,0)$ and vice versa are presented in Figure 10. The modulus of these conversion coefficients are found to remain lower than 0.1. Near the cut-off frequencies of modes $(1,0)$, $(2,0)$ and $(0,1)$ discontinuities occur. Theoretically, as the geometry

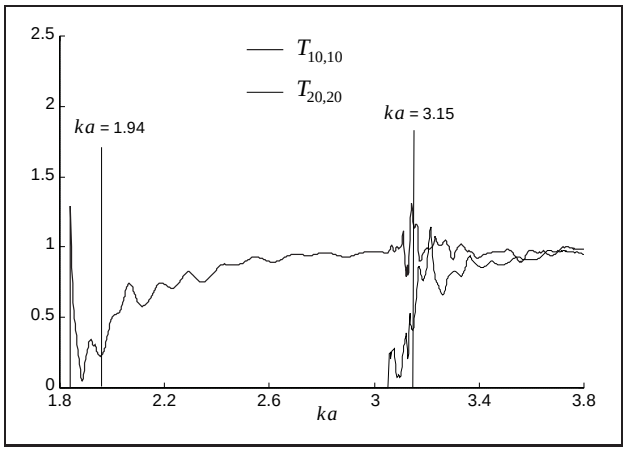

Figure 12. Modulus of the transmission coefficients $T_{10,10}$, $T_{20,20}$ versus ka.

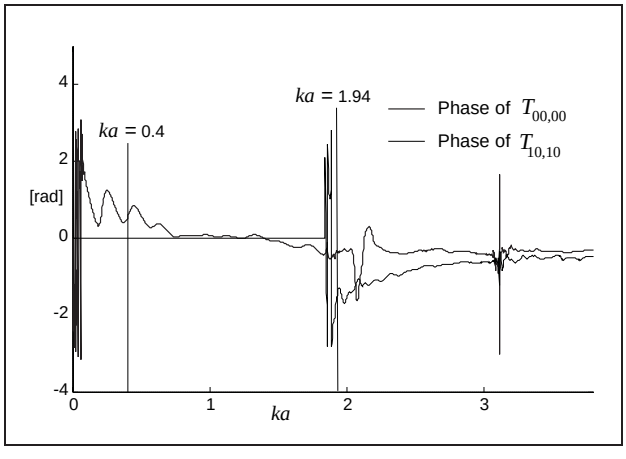

Figure 13. Phases of transmission coefficients $T_{00,00}$ and $T_{10,10}$ versus ka in $z = z_I$.

is assumed to be axisymetric, no conversion between azimuthal modes can occur. This experimental result points out that the actual geometry is not perfectly axisymetric or gives an estimation of the minimum level for the measurement of the modulus of a coefficient of matrix $[R]$.

3.3.2. Results of the measurement of the matrix $[T]$

The measured modulus of the plane wave transmission coefficient $T_{00,00}$ is shown in Figure 11. The condition equation (22) applies also to the measurement of transmission coefficients and the value of ka limit is marked in Figure 11. Values are close to one except for ka between 1 and 2 where the modulus of $T_{00,00}$ is decreasing from 1 to 0,75. This discrepancy is due to the measurement problem in section 2 caused by the stationary waves, as discussed before in section 2.3.1. The results of the modulus of the transmission coefficients $T_{10,10}$, $T_{20,20}$ of modes $(1,0)$, $(2,0)$ are shown in Figure 12. Values are converging to 1 when the frequency increases away from the cut-off frequency.

The phases of the transmission coefficients $T_{00,00}$ and $T_{10,10}$ are calculated in the same axial location z_I, and results are plotted in Figure 13 versus ka. The phase differ-

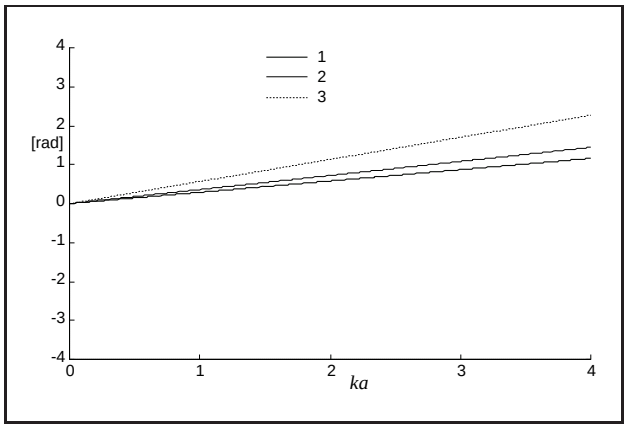

Figure 14. 1: Effect of uncertainties on distance z and temperature Γ on phase measurement of $T_{00,00}$ in $z = z_I$ (1: $\Delta z/z = 1\%$, $\Delta\Gamma/\Gamma = 5\%$; 2: $\Delta z/z = 1\%$, $\Delta\Gamma/\Gamma = 10\%$; 3: $\Delta z/z = 2\%$, $\Delta\Gamma/\Gamma = 5\%$).

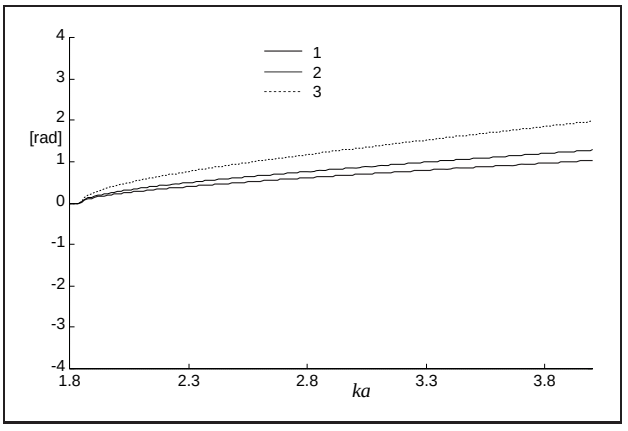

Figure 15. 1: Effect of uncertainties on distance z and temperature Γ on phase measurement of $T_{10,10}$ in $z = z_I$ (1: $\Delta z/z = 1\%$, $\Delta\Gamma/\Gamma = 5\%$; 2: $\Delta z/z = 1\%$, $\Delta\Gamma/\Gamma = 10\%$; 3: $\Delta z/z = 2\%$, $\Delta\Gamma/\Gamma = 5\%$).

ence between incident and transmitted waves are, as expected, nearly equal to zero except near cut-on frequencies. The curves point out slow phase variations with ka which are due to the uncertainties in distance estimation and temperature as shown in the curves presented in Figure 14 for plane wave and Figure 15 for mode $(1, 0)$. Indeed, a phase shift of about $\pi/3$ is produced by an error in z estimation of 1%.

Results of the modulus of the transmission conversion coefficients $T_{10,00}$, $T_{00,10}$ are shown in Figure 16. Except near cut-off frequencies, the values are lower than 0.05. The assumption on the axi-symetry is verified.

3.3.3. Results of acoustic power and attenuation

For each of the 6 source configurations, the total acoustic power in measurement sections I and II and the attenuation produced by the test duct were deduced from equations (15), (16) and (17). The mean value and the standard deviation of the attenuation on total acoustic power are deduced from equation (18) and equation (19). Results are plotted versus ka in Figure 17.

Theoretically, total acoustic power is conserved between sections I and II because the test section does not contain any dissipative element. As the standard deviation remains lower than 1 dB (Figure 17), the effect of source configuration is insignificant in the measurement of attenuation.

The power attenuation ΔW is very large near the cut-off frequencies of modes and reaches 2 dB for ka between 1 and 2. This discrepancy is issued from errors in measurement produced by the stationary waves in element II. From equation (15) and equation (16), for the plane wave case, ΔW can be written as

$$\Delta W = 10 \log \left(\frac{1 - |R^{II}_{00,00}|^2}{1 - |R^{I}_{00,00}|^2} \frac{1}{|T_{00,00}|^2} \right). \qquad (23)$$

As the duct element tested is a hard walled duct without discontinuity, theoretically $|R^{I}_{00,00}| = |R^{II}_{00,00}|$ and

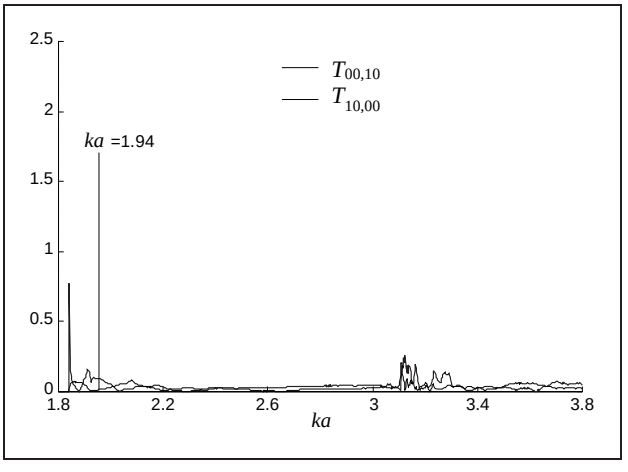

Figure 16. Modulus of the transmission conversion coefficients $T_{00,10}$ and $T_{10,00}$ versus ka.

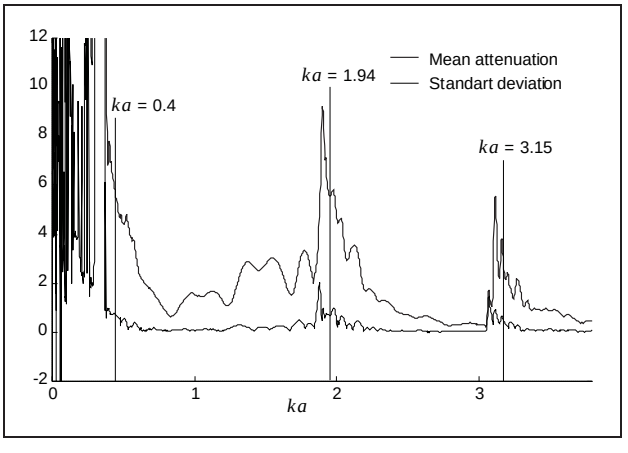

Figure 17. Mean value and standard deviation of the attenuation on total acoustic power, in dB, versus ka.

$|T_{00,00} = 1|$, then $\Delta W = 0$ dB. Let ΔR be the difference in the reflection coefficient measured in elements I and II and ΔT the error in the transmission coefficients:

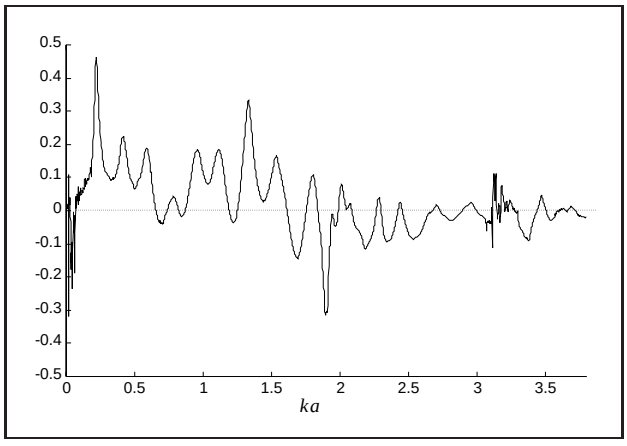

Figure 18. $\Delta R = |R^I_{00,00}| - |R^{II}_{00,00}|$ versus ka.

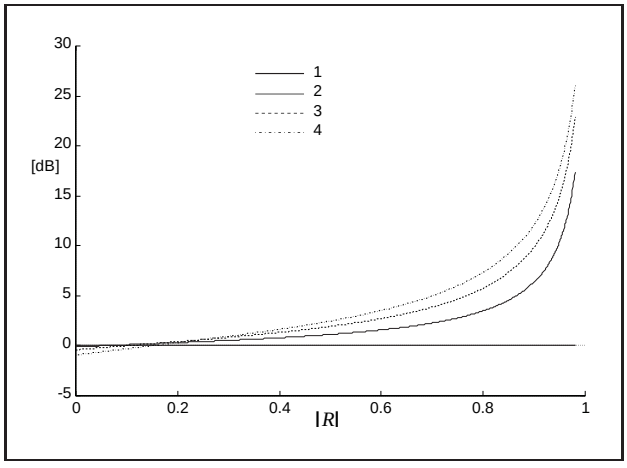

Figure 19. Effect of reflection coefficient uncertainties on acoustic power attenuation versus $|R^I_{00,00}|$ ($\Delta T = 0$, 1: $\Delta R = 0$; 2: $\Delta R = 0.1$; 3: $\Delta R = 0.2$; 4: $\Delta R = 0.3$).

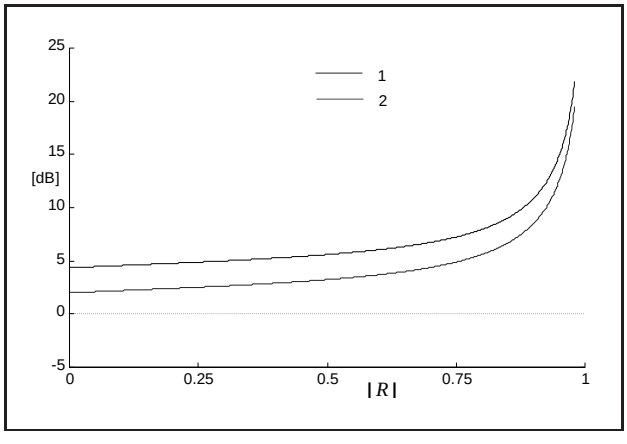

Figure 20. Effect of transmission coefficient uncertainties on acoustic power attenuation versus $|R^I_{00,00}|$ ($\Delta R = 0.1$, 1: $\Delta T = 0.1$; 2: $\Delta T = 0.2$).

$|R^{II}_{00,00}| = |R^I_{00,00}| \pm \Delta R$ and $|T_{00,00}| = 1 \pm \Delta T$, equation (23) becomes

$$\Delta W = 10 \log \left(\frac{1 - |R^I_{00,00} \pm \Delta R|^2}{1 - |R^I_{00,00}|^2} \frac{1}{|1 \pm \Delta T|^2} \right). \quad (24)$$

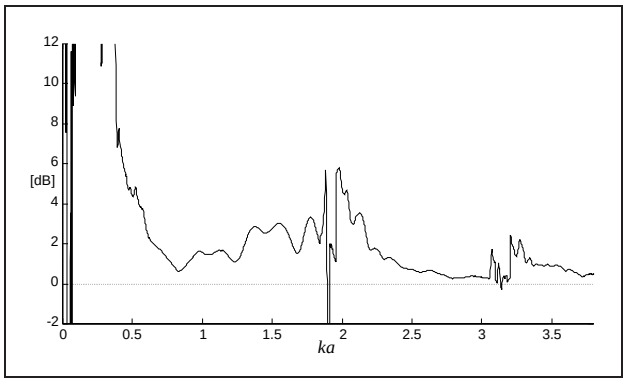

Figure 21. Modified acoustic power attenuation versus ka.

ΔW represents the error in the measurement of the attenuation. If the ka domain where the condition equation (22) is not satisfied, is excluded, ΔR versus ka varies from -0.3 to 0.3 as shown in Figure 18. Curves ΔW plotted versus $|R^I_{00,00}|$ in Figure 19 for several values of ΔR from 0 to 0.3 show that the error on ΔW produced by ΔR is higher than 10 dB when $|R|$ is higher than 0.85. Curves ΔW plotted versus $|R^I_{00,00}|$ in Figure 20 for $\Delta R = 0.1$ and for several values of ΔT from 0 to 0.2 (the maximum value deduced from the curve in Figure 11) show that the error in ΔW produced by ΔT is significant for low values of $|R^I_{00,00}|$.

To avoid the effect of modes near the cut-on frequency, the attenuation was deduced from equation (18), but excluding the contribution of a cut-on mode (m, n) for frequencies which satisfy equation (22). The result of the computation of this modified acoustic power attenuation is shown in Figure 21.

4. Conclusions

An experimental facility with an automatic procedure of collecting data was achieved to measure reflection matrices, transmission matrices, per mode or total acoustic power and acoustic power attenuation of a duct discontinuity in higher order modes' propagation conditions. An experiment was conducted on a duct without any discontinuity.

The results of measurement of the refection and conversion coefficients $R_{mn,pq}$ confirm those published in [5] and point out that

- the sound intensity probe improves the measurement:
  - avoiding the diffraction effect by the probe,
  - reducing near the cut-on frequency the upper frequency domain where errors occur.
- the location of the measurement section is an important parameter which can contribute to increased errors. The effect of this parameter can be limited by increasing the number of samples during the acquisition process and by attaching an anechoic termination to the end of the duct to reduce the axial standing wave.

The results of measurement of $T_{mn,pq}$ where incident and transmitted pressures are determined in the same z

axis position, agree with what is expected for a hard walled test element with no discontinuity:

- modulus close to 1,
- phase close to 0,
- small modulus conversion coefficients.

But errors happen in the same frequency bands as for the reflection coefficient, including the effect produced by the measurement in element II. The conservation law of acoustic power through the hard walled duct is verified except in the same frequency bands where errors in reflection and transmission coefficients are present. It is shown that to reduce these errors on the measurement of power attenuation, the accuracy in the reflection coefficient measurement should be increased, the more important its modulus is.

References

[1] E. R. Rademaker et al.: Publishable synthesis report Report DUCAT-NL-01.

[2] M. C. Munjal: Acoustics of ducts and mufflers. John Wiley, New York, 1987.

[3] J. Y. Chung, D. A. Blaser: Transfer function method for measuring in-duct acoustic properties. I. Theory, II. Experiment. Journal of the Acoustical Society of America **68** (1980) 907–921.

[4] M. Abom: Modal decomposition in ducts based on transfer function measurements between microphones pairs. Journal of Sound and Vibration **135** (1989) 95–114.

[5] M. Akoum, J. M. Ville: Measurement of the reflection matrix of a discontinuity in a duct. Journal of the Acoustical Society of America **103** (1998) 2463–2468.

[6] M. Abom: Measurement of the scattering matrix of acoustical two-ports. Mechanical Systems and Signal Processing **5** (1991) 89–104.

[7] P. M. Morse, K. U. Ingard: Theoretical acoustics. McGraw-Hill, New York, 1968.

[8] J. M. Auger, J. M. Ville: Measurement of liner impedance based on determination of duct eigenvalues by a Fourier-Lommel's transform. Journal of the Acoustical Society of America **88** (1990) 19–22.

[9] M. Abom, H. Boden: Error analysis of two microphones measurements in ducts with flow. Journal of the Acoustical Society of America **83** (1988) 2429–2438.

[10] W. Neise, F. Arnold: On sound power determination in flow ducts. Journal of Sound and Vibration **244** (2001) 481–503.